Chemical Engineering Science 63 (2008) 3152 – 3159

Contents lists available at ScienceDirect

Chemical Engineering Science

journal homepage: www.elsevier.com/locate/ces

Re-evaluation of the Nusselt number for determining the interfacial heat and mass transfer coefficients in a flow-through monolithic catalytic converter

Tae Joong Wang[a,*], Seung Wook Baek[a], Sung Jin Kim[b]

[a]Propulsion and Combustion Laboratory, School of Mechanical, Aerospace and Systems Engineering, Korea Advanced Institute of Science and Technology (KAIST), 373-1 Guseong-dong, Yuseong-gu, Daejeon 305-701, Republic of Korea

[b]Applied Heat Transfer Laboratory, School of Mechanical, Aerospace and Systems Engineering, Korea Advanced Institute of Science and Technology (KAIST), 373-1 Guseong-dong, Yuseong-gu, Daejeon 305-701, Republic of Korea

ARTICLE INFO

Article history:
Received 21 August 2007
Received in revised form 23 January 2008
Accepted 21 March 2008
Available online 27 March 2008

Keywords:
Heat transfer
Mass transfer
Numerical analysis
Porous media
Catalytic converter
Nusselt number

ABSTRACT

The two-equation porous medium model has been widely employed for modeling the flow-through monolithic catalytic converter. In this model, the interfacial heat and mass transfer coefficients have been usually obtained using the asymptotic Nusselt and Sherwood numbers with some suitable assumptions. However, previously it seemed that there existed some misunderstanding in adopting these Nusselt and Sherwood numbers. Up to now, the Nusselt number based on the fluid bulk mean temperature has been used for determining the interfacial heat and mass transfer coefficients. However, the mass and energy balance formulations in the two-equation model indicate that the Nusselt number should be evaluated based on the fluid mean temperature instead of the fluid bulk mean temperature. Therefore, in this study, to correctly model the heat and mass transfer coefficients, the Nusselt number based on the fluid mean temperature was newly obtained for the square and circular cross-sections under two different thermal boundary conditions (i.e., constant heat flux and constant temperature at the wall). In order to do that, the present study employed the numerical as well as analytical method.

1. Introduction

As a part of efforts to reduce exhaust emissions from vehicles, the use of flow-through type monolithic catalytic converters has been substantially increased during the past several decades. As world-wide automobile emission legislations become tighter, its technology is also developing so fast. In order to reduce developing cost in experiments, the numerical modeling is in high demand for the analysis and design.

In modeling the catalytic converter, the porous medium approach has been widely adopted while considering the trade-offs between cost and accuracy. Most of previous works have employed the two-equation model, in which gas phase (i.e., exhaust flow) and solid phase (i.e., catalyst/washcoat and substrate) are, respectively, viewed as individually continuous medium. Thereby, the phase-averaged solution is obtained for each phase (Kaviany, 1995; Quintard and Whitaker, 2000).

In the two-equation porous medium model, interfacial heat and mass transfer coefficients are crucial factors which describe linkages between gas and solid phases. These coefficients have been mostly obtained using asymptotic Nusselt and Sherwood numbers with some proper assumptions. Several Nusselt numbers employed in the literatures are summarized in Table 1. Note that it is enough to utilize only the Nusselt number for obtaining both transfer coefficients because Sherwood number is assumed to be the same as Nusselt number from the heat and mass transfer analogy, which implies that if the bulk flow configuration is the same in both problems and if the wall boundary condition is the same, the mass transfer result can be obtained directly from the heat transfer result (Bejan, 1995).

The values listed in Table 1 were originated from the following earlier works. For a square channel, Clark and Kays (1953) presented fully developed Nusselt numbers for different boundary conditions using the finite difference method. The reported value is 3.63 under the axially constant heat transfer rate per unit length with constant peripheral wall temperature (**H1** boundary condition), while 2.89 under the uniform wall temperature peripherally as well as axially (**T** boundary condition). More refined finite difference solutions are given in Shah and London (1978) such that 3.60795 for **H1** and 2.976 for **T**. For a round channel, there exists an analytic solution of 48/11 for **H1** (Incropera and DeWitt, 2002; Shah and London, 1978), while an infinite series solution of 3.6567935 is reported for **T** (Shah and London, 1978).

* Corresponding author. Tel: +82 42 869 3754; fax: +82 42 869 3710.
E-mail address: cakecandle@kaist.ac.kr (T. J. Wang).

0009-2509/$ - see front matter © 2008 Elsevier Ltd. All rights reserved.
doi:10.1016/j.ces.2008.03.027

Table 1
Asymptotic Nusselt and Sherwood numbers generally employed in the literatures to determine the interfacial heat and mass transfer coefficients

References	Asymptotic Nusselt and Sherwood number
Siemund et al. (1996), Jeong and Kim (2000)	2.89
Chen and Cole (1989)	2.982
Taylor (1999)	2.97
Keren and Sheintuch (2000)	3.66

However, it seemed that there were previously some mistakes in applying the Nusselt numbers to obtain interfacial heat and mass transfer coefficients. Until now, all the asymptotic Nusselt numbers adopted in the earlier works have been based on the fluid bulk mean temperature. However, according to the two-equation model formulation in those works, the Nusselt numbers should be based on the fluid mean temperature, not on the fluid bulk mean temperature. In order to correct this error, the current study first provides some discussions on the formulation of the two-equation model together with appropriate Nusselt numbers, and then newly derives the Nusselt numbers based on the fluid mean temperature using the numerical as well as the analytical method for circular and square cross-sections under **H1** and **T** boundary conditions. Particularly regarding the solution method, the present work employs the non-dimensional technique as in Clark and Kays (1953).

2. General formulations on the catalytic converter

According to the literatures employing the two-equation porous medium approach to model the cylindrical automobile catalytic converters such as Chen et al. (1988), Guojiang and Song (2005), Keren and Sheintuch (2000), Koltsakis and Stamatelos (1997), Oh and Cavendish (1982), and Zygourakis (1989), typical differential equations describing the mass and energy transport between two phases can be expressed in two-dimensional axisymmetric domain as follows:

Gas phase mass balance equation for species i:

$$\varepsilon\frac{\partial C_{g,i}}{\partial t} = -\varepsilon u_g\frac{\partial C_{g,i}}{\partial x} - k_{m,i}a_{sf}(C_{g,i} - C_{s,i}). \tag{1}$$

Solid phase mass balance equation for species i:

$$(1-\varepsilon)\frac{\partial C_{s,i}}{\partial t} = k_{m,i}a_{sf}(C_{g,i} - C_{s,i}) - a_c\sum R_i. \tag{2}$$

Gas phase energy balance equation:

$$\varepsilon\rho_g c_{p,g}\frac{\partial T_g}{\partial t} = -\varepsilon\rho_g c_{p,g}u_g\frac{\partial T_g}{\partial x} + h_{sf}a_{sf}(T_s - T_g). \tag{3}$$

Solid phase energy balance equation:

$$(1-\varepsilon)\rho_s c_{p,s}\frac{\partial T_s}{\partial t} = (1-\varepsilon)k_{s,x}\frac{\partial^2 T_s}{\partial x^2} + (1-\varepsilon)k_{s,r}\frac{1}{r}\frac{\partial}{\partial r}\left(r\frac{\partial T_s}{\partial r}\right) - h_{sf}a_{sf}(T_s - T_g) + a_c\sum(-\Delta H_i)R_i. \tag{4}$$

The above formulation set of Eqs. (1)–(4) resulted from the intrinsic phase-averaging for the general form of conservation equations. Each primitive variable (i.e., C_g, C_s, T_g, and T_s) and u_g represent the intrinsic phase-averaged quantities defined as (Nield and Bejan, 1992; Quintard and Whitaker, 2000)

$$\phi_\alpha \equiv \frac{1}{V_\alpha}\int_{V_\alpha}\phi\,\mathrm{d}V, \tag{5}$$

where α means the phase (i.e., gas or solid).

In order to describe the channel flow configuration, the Darcy flow model or the fully developed laminar flow model has been usually employed. The Darcy flow model (Bejan, 1995; Kaviany, 1995; Nield and Bejan, 1992) assumes that the flow has a uniform velocity profile over the channel cross-section so that no slip condition does not hold at the wall. Here, since the axial velocity can be easily obtained from the Darcy law; $u_D = K/\mu(-\mathrm{d}P/\mathrm{d}x)$, the momentum equation is not required to be solved. Note in this model that the Nusselt numbers presented in Table 1 cannot be used because they are obtained under the fully developed laminar flow assumption. Actually, the Nusselt numbers for the Darcy flow are larger than those for the fully developed laminar flow. Refer to the values produced by Asako et al. (1988) for the slug flow (i.e., longitudinally uniform over the cross-section) in several cross-sections. For a physical viewpoint, the fully developed laminar flow model is more realistic one. In this model, local velocities are known for several simple cross-section geometries so that the phase-averaged velocity present in Eqs. (1) and (3) can be obtained from their integration. In actual problems, it is easily estimated using the simple relation, $u_g = Q/A_p$ with the known intake volumetric flow rate. Therefore, as for the Darcy flow model, it is not necessary to solve the momentum equation here. Note that, although Eqs. (1) and (3) are expressed as an one-dimensional form, they are not physically one-dimensional.

There are possibly two options depending on the region of the intrinsic phase-averaging. First, the averaging is carried out over the entire monolith cross-section, which yields one-dimensional velocity and concentrations all over the monolith. Second, the averaging is performed for each channel and then Eqs. (1)–(3) are solved line by line along radial direction. This gives multi-dimensional velocity and concentrations over the monolith. Note that, for both cases, the solid temperature can be obtained multi-dimensionally.

3. Proposing new Nusselt number

In the formulation set from Eqs. (1) to (4), one of the most important tasks is how to obtain the interfacial transfer coefficients for heat, h_{sf} and mass of ith species, $k_{m,i}$. Meanwhile, these two coefficients have been usually determined through the following way.

First, h_{sf} is calculated from the definition of Nusselt number as

$$Nu \equiv \frac{h_{sf}d_h}{k_g}, \tag{6}$$

where the Nusselt number is usually assumed to be a constant. Its theoretical background is that, for a circular or square channel whose cross-section shape does not change axially, the Nusselt number approaches an asymptotic value as the flow becomes thermally fully developed under **H1** or **T** boundary condition. Here, the flow is assumed to be already hydrodynamically fully developed, which is reasonable because the Prandtl number of exhaust gases from vehicles has a near unity and thereby the hydrodynamic and thermal entrance lengths are in the same order of magnitude. In addition, for real-world vehicle operating conditions, the hydrodynamic entrance length is very short. For example, if an air at 600 K passes through a monolith of 400/6.5 (cell density [cells/in^2]/wall thickness [m in]) configuration with 0.11 m outer-diameter at 20 l/s volumetric flow rate, the single channel Reynolds number based on the fluid mean velocity becomes approximately 43.9. Referring to Wiginton and Dalton (1970) in which the dimensionless length defined by $L_{hy}/(d_h\,Re)$ is reported to 0.09, the hydrodynamic entrance length is calculated to about 4.3 mm.

Second, $k_{m,i}$ is obtained from the definition of Sherwood number as

$$Sh \equiv \frac{k_{m,i}d_h}{D_i}, \tag{7}$$

where the Sherwood number is assumed to be the same as the Nusselt number using the heat and mass transfer analogy.

So far, the asymptotic Nusselt numbers adopted in the literatures have been evaluated based on the fluid bulk mean temperature as follows:

$$Nu_b \equiv \frac{d_h q''}{k_g(T_s - T_m)}. \tag{8}$$

In Eq. (8), the fluid bulk mean temperature is defined as

$$T_m \equiv \frac{1}{u_m A_p} \int_{A_p} uT \, dA, \tag{9}$$

where the fluid mean axial velocity is defined as

$$u_m \equiv \frac{1}{A_p} \int_{A_p} u \, dA. \tag{10}$$

The above Eq. (8) implies that the heat transfer between gas and solid phases is derived by the difference in the solid wall temperature and the fluid bulk mean temperature as follows:

$$q'' = h(T_s - T_m). \tag{11}$$

However, the fluid temperature, T_g present in Eqs. (3) and (4) does not indicate the fluid bulk mean temperature, instead it represents the fluid mean temperature (i.e., intrinsic phase-averaged temperature). That is, in the two-equation porous medium model, the heat transfer between phases should be described by the difference of the solid wall temperature and the fluid mean temperature as

$$q'' = h_{sf}(T_s - T_g), \tag{12}$$

where the fluid mean temperature is defined by

$$T_g \equiv \frac{1}{A_p} \int_{A_p} T \, dA. \tag{13}$$

Consequently, Eq. (12) suggests that the Nusselt number used for determining the interfacial heat transfer coefficient should be evaluated based on the fluid mean temperature as follows:

$$Nu \equiv \frac{d_h q''}{k_g(T_s - T_g)}. \tag{14}$$

4. Obtaining the Nusselt number based on the fluid mean temperature

This section provides a detailed procedure to calculate the Nusselt numbers for the simplified cross-section shapes (i.e., circular and square) with the idealized thermal boundary conditions (i.e., **H1** and **T**). A sample picture of an actual channel cross-section of a commercial monolithic catalytic converter is displayed in Fig. 1, which shows that the shape of the pore is not exactly a square or circle. However, for simplicity, most of the modeling works have regarded the pore as a square, while Keren and Sheintuch (2000) considered it as a circle. Inspection of the values listed in Table 1 reveals that the literatures mostly refer to the Nusselt and Sherwood numbers obtained for **T**. Nevertheless, for extension, this study accounts for both **H1** and **T**. For a heat exchanger with highly conductive materials (i.e., copper and aluminum), the **H1** may apply. However, it may be difficult to achieve this boundary condition for non-circular ducts. The **T** boundary condition is realized in many practical applications such as condensers, evaporators, and automotive radiators having high liquid flow rates (Shah and London, 1974, 1978).

In order to obtain the velocity and temperature fields yielding the asymptotic Nusselt number, the current study derives the partial differential form of momentum and energy equations with the following assumptions.

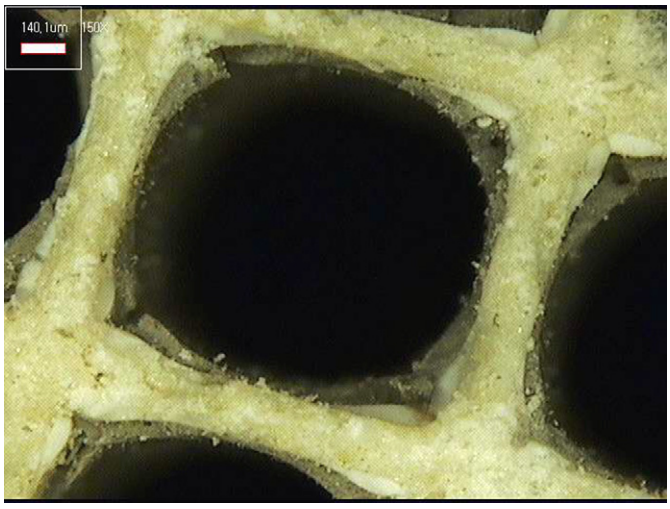

Fig. 1. High-magnification microscope photograph of the substrate and catalyst layer in a commercial diesel oxidation catalyst (×150). The cell density is 400 cells/in^2 and the substrate wall thickness is 6.5 m in.

- The shape of the channel cross-section does not change axially.
- Flow is laminar and is fully developed thermally as well as hydrodynamically.
- Thermo-physical fluid properties such as density, specific heat, dynamic viscosity, and thermal conductivity are constant.
- Heat conduction in the direction of flow is negligible.
- Conversion of mechanical to thermal energy due to friction is negligible relative to the heat transfer.
- Natural convection effect is negligible.

Justifications of the above assumptions can be reviewed in several heat transfer text books (Bejan, 1995; Kays and Crawford, 1993).

4.1. Square channel

Using the previous assumptions, the governing momentum and energy equations for the square channel can be written as follows:

$$\frac{\partial^2 u}{\partial y^2} + \frac{\partial^2 u}{\partial z^2} = \frac{1}{\mu}\frac{dP}{dx}, \tag{15}$$

$$\frac{\partial^2 T}{\partial y^2} + \frac{\partial^2 T}{\partial z^2} = \frac{u}{\alpha}\frac{\partial T}{\partial x}. \tag{16}$$

For the square cross-section, an analytic solution for the momentum equation is available in the form of an infinite series (Shah and London, 1978), while there is no analytic solution for the energy equation. Nevertheless, the current study numerically solves both equations because the analytic solution involves considerable computational complexities. In addition, since two equations are in the same type (i.e., Poisson's equation) as well as in the same order, almost no additional cost arises. The solution of the energy equation is dependent on the thermal boundary condition, whereas the momentum equation is independent of it. Thus, the momentum equation is solved first. The solutions of Eqs. (15) and (16) are obtained only for a quarter of the cross-section. Then, from symmetry, all the fields can be known. A schematic representation of the computational domain is illustrated in Fig. 2.

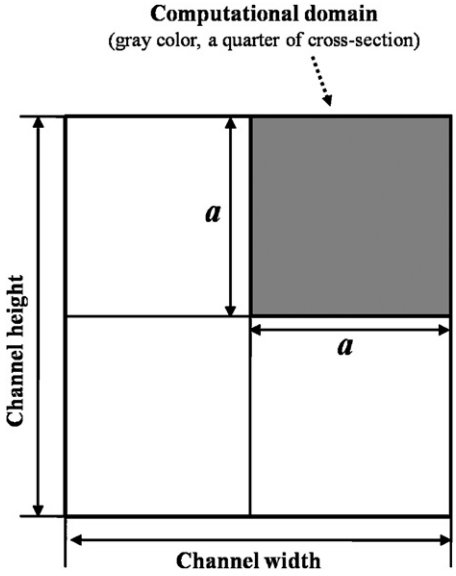

Fig. 2. Schematic view of a computational domain of square channel.

As the first step to get the velocity field, Eq. (15) is discretized using the second-order central difference scheme as follows:

$$\frac{u_{i+1,j}-2u_{i,j}+u_{i-1,j}}{(\Delta z)^2}+\frac{u_{i,j+1}-2u_{i,j}+u_{i,j-1}}{(\Delta y)^2}=\frac{1}{\mu}\frac{\mathrm{d}P}{\mathrm{d}x}. \tag{17}$$

Here, the computational domain is divided into $N\times N$ grid system and the grid interval in each direction is set to be equal such that $\Delta y=\Delta z=a/N$. At this point, a non-dimensional velocity is introduced as

$$u^*=\frac{u}{\frac{a^2}{\mu}\left(-\frac{\mathrm{d}P}{\mathrm{d}x}\right)}. \tag{18}$$

Then, Eq. (17) can be rearranged non-dimensionally as follows:

$$u^*_{i-1,j}+u^*_{i,j-1}-4u^*_{i,j}+u^*_{i+1,j}+u^*_{i,j+1}=-\frac{1}{N^2}. \tag{19}$$

On each grid point, Eq. (19) was solved with no slip condition at the wall. The grid system used was 400×400. The strongly implicit procedure (SIP) proposed by Stone (1968) was adopted as the solution algorithm.

Fig. 3 shows the calculated non-dimensional axial velocity field within a quarter of the square channel. For verifying the result, the $f\,Re$ factor is calculated as

$$f\,Re=\frac{\frac{2a^2}{\mu}\left(-\frac{\mathrm{d}P}{\mathrm{d}x}\right)}{u_m}=\frac{2}{u^*_m}, \tag{20}$$

where the non-dimensional fluid mean velocity is defined by

$$u^*_m\equiv\frac{1}{A_p}\int_{A_p}u^*\,\mathrm{d}A. \tag{21}$$

The currently obtained $f\,Re$ is 14.22715, which shows a good agreement with 14.22708 reported by Shah and London (1978).

4.1.1. *H1 boundary condition*

For this boundary condition, the axial temperature gradient term on the right hand side of Eq. (16) becomes (Bejan, 1995; Clark and Kays, 1953, Kays and Crawford, 1993)

$$\frac{\partial T}{\partial x}=\frac{\mathrm{d}T_s}{\mathrm{d}x}=\frac{\mathrm{d}T_m}{\mathrm{d}x}=\text{constant}. \tag{22}$$

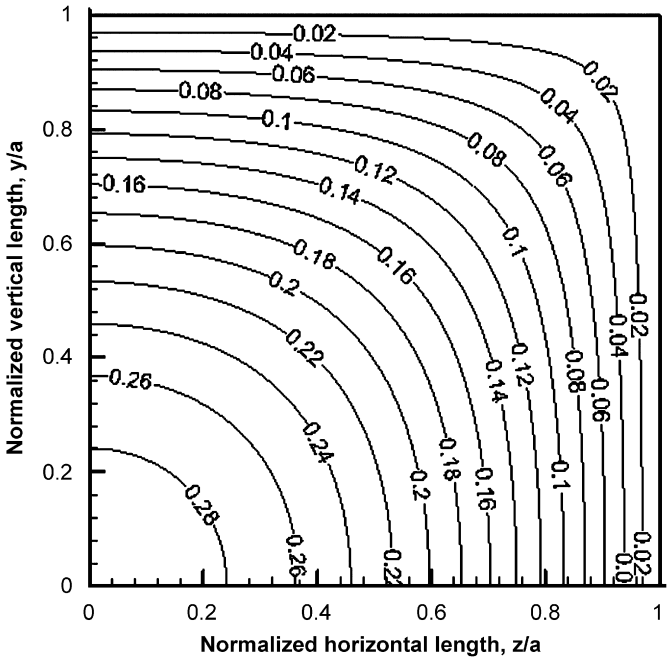

Fig. 3. Non-dimensional axial velocity contour within a quarter of square cross-section.

Discretizing Eq. (16) yields

$$\frac{T_{i+1,j}-2T_{i,j}+T_{i-1,j}}{(\Delta z)^2}+\frac{T_{i,j+1}-2T_{i,j}+T_{i,j-1}}{(\Delta y)^2}=\frac{u_{i,j}}{\alpha}\frac{\mathrm{d}T_m}{\mathrm{d}x}. \tag{23}$$

By introducing such non-dimensional temperature as

$$T^*=\frac{T}{\frac{a^4}{\alpha\mu}\left(-\frac{\mathrm{d}P}{\mathrm{d}x}\right)\left(\frac{\mathrm{d}T_m}{\mathrm{d}x}\right)}. \tag{24}$$

Eq. (23) can be rearranged non-dimensionally as follows:

$$T^*_{i-1,j}+T^*_{i,j-1}-4T^*_{i,j}+T^*_{i+1,j}+T^*_{i,j+1}=\frac{u^*_{i,j}}{N^2}. \tag{25}$$

Then, the following boundary condition is implemented.

$$T^*|_{wall}=1.0. \tag{26}$$

Eq. (25) was solved with substituting the previously obtained velocity field into its source term. The calculated non-dimensional temperature field is illustrated in Fig. 4. Also, the non-dimensional mean temperatures are introduced as follows:

$$T^*_m\equiv\frac{1}{u^*_m A_p}\int_{A_p}u^*T^*\,\mathrm{d}A, \tag{27}$$

$$T^*_g\equiv\frac{1}{A_p}\int_{A_p}T^*\,\mathrm{d}A. \tag{28}$$

From Eqs. (27) and (28), T^*_m is calculated to 0.961037, while T^*_g is 0.972760.

By applying the energy conservation to an axially infinitesimal volume, the Nusselt number based on the fluid bulk mean temperature is evaluated as (Shah, 1975)

$$Nu_b=\frac{d_h(q'/L_p)}{k_g(T_s-T_m)}=\frac{d_h}{L_p}\frac{A_p}{\alpha}\frac{\mathrm{d}T_m}{\mathrm{d}x}\frac{u_m}{T_s-T_m}=\frac{u^*_m}{T^*_s-T^*_m}. \tag{29}$$

Eq. (29) yields Nu_b to 3.607947, which is almost the same value as 3.60795 reported by Shah and London (1978). On the other hand, the

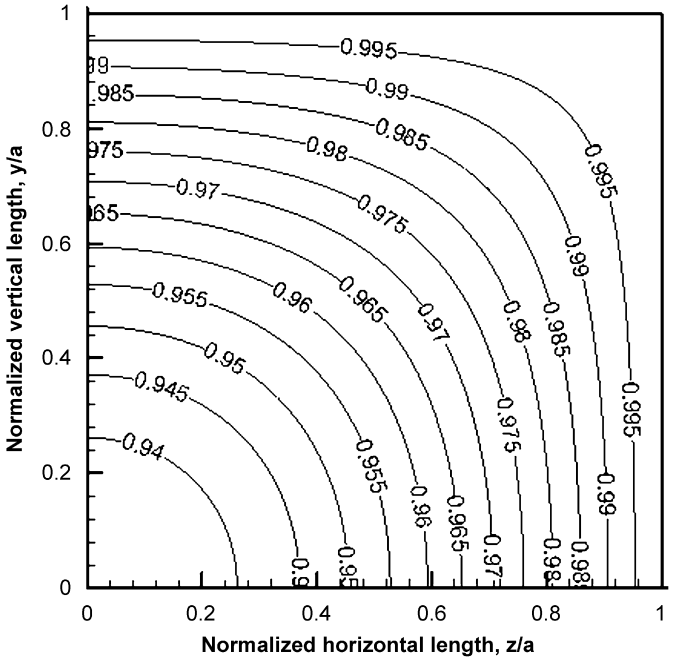

Fig. 4. Non-dimensional temperature contour within a quarter of square cross-section for the **H1** boundary condition.

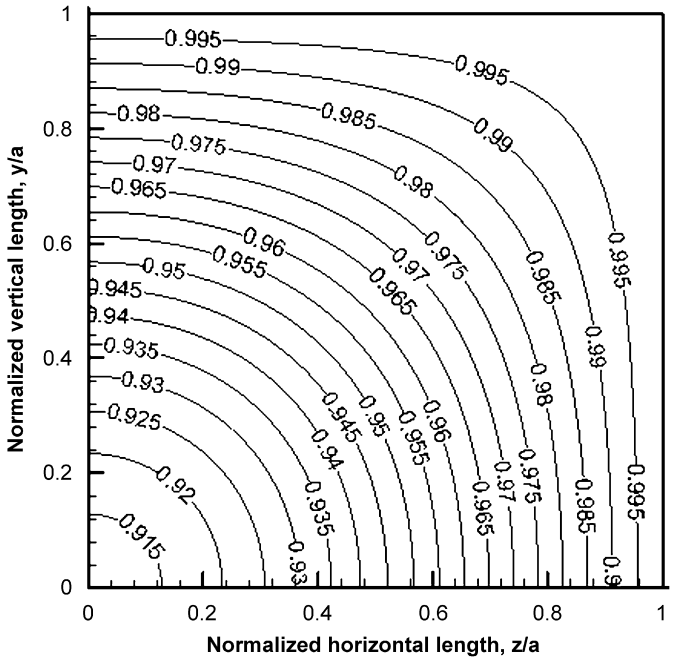

Fig. 5. Non-dimensional temperature contour within a quarter of square cross-section for the **T** boundary condition.

Nusselt number based on the fluid mean temperature is obtained from

$$Nu = \frac{d_h(q'/L_p)}{k_g(T_s - T_g)} = \frac{d_h}{L_p}\frac{A_p}{\alpha}\frac{\mathrm{d}T_m}{\mathrm{d}x}\frac{u_m}{T_s - T_g} = \frac{u_m^*}{T_s^* - T_g^*}. \tag{30}$$

Eq. (30) yields *Nu* to 5.160639, which is absolutely different from the above Nu_b. Consequently, this newly obtained *Nu* is proposed to be used for determining the interfacial heat and mass transfer coefficients in the forthcoming two-equation porous medium model of catalytic converters having square channels under **H1**.

*4.1.2. **T** boundary condition*

With this boundary condition, the axial temperature gradient term of Eq. (16) becomes (Bejan, 1995; Clark and Kays, 1953; Kays and Crawford, 1993)

$$\frac{\partial T}{\partial x} = \frac{T_s - T}{T_s - T_m}\frac{\mathrm{d}T_m}{\mathrm{d}x}. \tag{31}$$

Substituting Eq. (31) into Eq. (16) and discretizing it yields

$$\frac{T_{i+1,j} - 2T_{i,j} + T_{i-1,j}}{(\Delta z)^2} + \frac{T_{i,j+1} - 2T_{i,j} + T_{i,j-1}}{(\Delta y)^2} = \frac{u_{i,j}}{\alpha}\frac{T_s - T_{i,j}}{T_s - T_m}\frac{\mathrm{d}T_m}{\mathrm{d}x}, \tag{32}$$

which can be represented in a non-dimensional form as follows:

$$T^*_{i-1,j} + T^*_{i,j-1} - 4T^*_{i,j} + T^*_{i+1,j} + T^*_{i,j+1} = \frac{u^*_{i,j}}{N^2}\frac{T_s^* - (T^*_{i,j})^p}{T_s^* - T_m^*}. \tag{33}$$

The same boundary condition as given in Eq. (26) is applied here for convenience in comparing the result with that of the previous **H1**. In order to solve Eq. (33) numerically, an iterative technique in which guessing and improving steps are continued until the solution converges is required since the dependent variables (i.e., non-dimensional local and bulk mean temperature) are in the source term. Note that, although the temperature at node (i, j) on the right hand side of Eq. (33) could be implicitly treated (i.e., transposing it into the left hand side), this induced a poor convergence. Therefore, the term was evaluated from the value at previous iteration step as denoted by the superscript, *p*. Here, the temperature field previously obtained for **H1** was used as the first estimation. By doing so, only several steps from this start were required to meet the following convergence criterion.

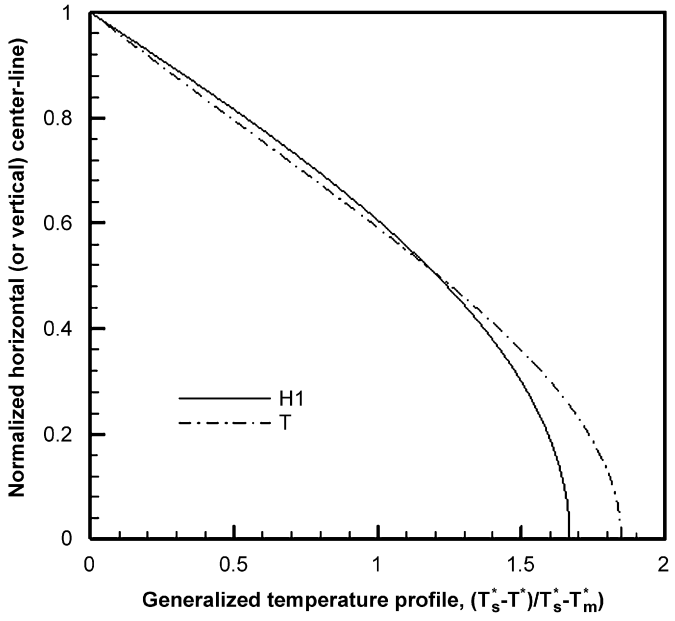

Fig. 6. Comparison of the generalized temperature profiles along the centerline of the square cross-section for the **H1** and **T** boundary conditions.

$$\left|\frac{\text{current } T_m - \text{previous } T_m}{\text{current } T_m}\right| < 1.0 \times 10^{-10}. \tag{34}$$

Fig. 5 shows the obtained non-dimensional temperature field for **T**. And, Fig. 6 illustrates a comparison of the generalized tempera-

ture profiles along the cross-section centerline for **H1** and **T**, which indicates that the profile for **H1** is more uniform than that of **T** as described in Kays and Crawford (1993). Also, from Eqs. (27) and (28), T_m^* is calculated to 0.952787 and T_g^* is 0.967912. Note that these two values are lower than those for **H1** counterparts. In addition, Nu_b is calculated to 2.977507, which differs only about 0.05% from 2.976 reported by Shah and London (1978). On the other hand, Nu is calculated to 4.380965, which is newly recommended to be used for the case of **T**.

4.2. Circular channel

For the circular channel, the governing momentum and energy equations are expressed as

$$\frac{1}{r}\frac{\partial}{\partial r}\left(r\frac{\partial u}{\partial r}\right)=\frac{1}{\mu}\frac{dP}{dx}, \tag{35}$$

$$\frac{1}{r}\frac{\partial}{\partial r}\left(r\frac{\partial T}{\partial r}\right)=\frac{u}{\alpha}\frac{\partial T}{\partial x}. \tag{36}$$

As can be seen from many heat transfer literatures, the well known Hagen–Poiseuille solution for Eq. (35) gives (Bejan, 1995; Incropera and DeWitt, 2002; Kays and Crawford, 1993)

$$u=2u_m\left[1-\left(\frac{r}{r_o}\right)^2\right], \tag{37}$$

$$u_m=\frac{r_o^2}{8\mu}\left(-\frac{dP}{dx}\right), \tag{38}$$

where r_o denotes the radius of a circular tube.

4.2.1. *H1* boundary condition

For this boundary condition, Nu_b is analytically calculated to 48/11 (Bejan, 1995; Incropera and DeWitt, 2002; Kays and Crawford, 1993; Shah and London, 1978). Then, Nu can be obtained from

$$Nu=Nu_b\frac{T_s-T_m}{T_s-T_g}. \tag{39}$$

The analytic solution for Eq. (36) gives (Incropera and DeWitt, 2002)

$$T=T_s-\frac{2u_m r_o^2}{\alpha}\left(\frac{dT_m}{dx}\right)\left[\frac{3}{16}-\frac{1}{4}\left(\frac{r}{r_o}\right)^2+\frac{1}{16}\left(\frac{r}{r_o}\right)^4\right] \tag{40}$$

$$T_m=T_s-\frac{11}{48}\left(\frac{u_m r_o^2}{\alpha}\right)\left(\frac{dT_m}{dx}\right) \tag{41}$$

Eqs. (13) and (40) lead to

$$T_g=\frac{1}{\pi r_o^2}\int_0^{r_o}T2\pi r\,dr=T_s-\frac{1}{6}\left(\frac{u_m r_o^2}{\alpha}\right)\left(\frac{dT_m}{dx}\right). \tag{42}$$

Inserting Eqs. (41) and (42) into Eq. (39) yields Nu to 6, which is proposed for the circular channel under **H1**. This result can be also obtained numerically. To verify the accuracy of the current numerical solution, the Nu is calculated again here. First, a non-dimensional velocity is introduced and rearranged using Eqs. (37) and (38) as

$$u^+=\frac{u}{\frac{r_o^2}{8\mu}\left(-\frac{dP}{dx}\right)}=2\left[1-\left(\frac{r}{r_o}\right)^2\right]. \tag{43}$$

Then, a non-dimensionalized fluid mean velocity becomes

$$u_m^+=\frac{u_m}{\frac{r_o^2}{8\mu}\left(-\frac{dP}{dx}\right)}=1. \tag{44}$$

Also, a non-dimensional temperature is introduced and rearranged using Eq. (40) as

$$T^+=\frac{T}{\frac{r_o^4}{8\alpha\mu}\left(-\frac{dP}{dx}\right)\left(\frac{dT_m}{dx}\right)}=T_s^+-2\left[\frac{3}{16}-\frac{1}{4}\left(\frac{r}{r_o}\right)^2+\frac{1}{16}\left(\frac{r}{r_o}\right)^4\right]. \tag{45}$$

In this case, referring Eq. (29), the non-dimensional expression of Nu_b becomes

$$Nu_b=\frac{1}{T_s^+-T_m^+}, \tag{46}$$

where

$$T_m^+\equiv\frac{1}{u_m^+A_p}\int_{A_p}u^+T^+\,dA. \tag{47}$$

Integrating Eq. (47) numerically and substituting it into Eq. (46) yields Nu_b to 4.363636357, which is almost the same as the analytic solution of 48/11. Here, for the computation, the radius of circular cross-section was divided into 40 000 grid points (i.e., $\Delta r=r_o/N=r_o/40\,000$).

Also, referring Eq. (30), the non-dimensional expression of Nu becomes

$$Nu=\frac{1}{T_s^+-T_g^+}, \tag{48}$$

where

$$T_g^+\equiv\frac{1}{A_p}\int_{A_p}T^+\,dA. \tag{49}$$

Integrating Eq. (49) numerically and substituting it into Eq. (48) yields Nu to 6.000000001, which shows almost no error in comparison with the exact solution of 6.

4.2.2. *T* boundary condition

Unlike the **H1** case, there is no analytic solution of the energy equation for **T** so that the numerical method is the only way to get the Nusselt number. By substituting Eqs. (31) and (37) into Eq. (36), the following form of the energy equation is solved for **T**.

$$\frac{\partial^2 T}{\partial r^2}+\frac{1}{r}\frac{\partial T}{\partial r}=\frac{2u_m}{\alpha}\frac{dT_m}{dx}\left[1-\left(\frac{r}{r_o}\right)^2\right]\frac{T_s-T}{T_s-T_m}. \tag{50}$$

Discretizing Eq. (50) yields

$$\frac{T_{i+1}-2T_i+T_{i-1}}{(\Delta r)^2}+\frac{1}{r_i}\frac{T_{i+1}-T_{i-1}}{2\Delta r}=\frac{2u_m}{\alpha}\frac{dT_m}{dx}\left[1-\left(\frac{r_i}{r_o}\right)^2\right]\frac{T_s-(T_i)^p}{T_s-T_m}, \tag{51}$$

which is rearranged non-dimensionally as

$$\left(1-\frac{1}{2N(r_i/r_o)}\right)T_{i-1}^+-2T_i^++\left(1+\frac{1}{2N(r_i/r_o)}\right)T_{i+1}^+=\frac{2}{N^2}\left[1-\left(\frac{r_i}{r_o}\right)^2\right]\frac{T_s^+-(T_i^+)^p}{T_s^+-T_m^+}. \tag{52}$$

Then, the following boundary condition is implemented.

$$T^+|_{wall}=T_s^+=1.0. \tag{53}$$

Identically to the solution procedure for the square cross-section, the iterative technique was adopted and the well known tri-diagonal

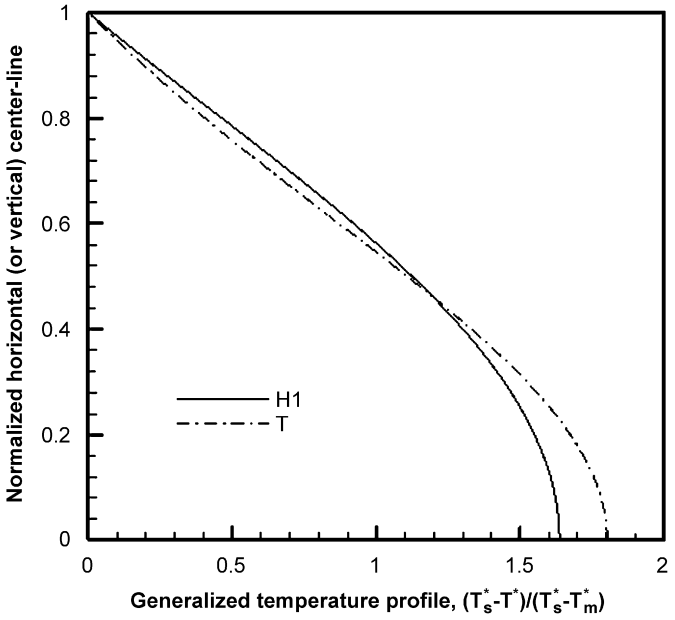

Fig. 7. Comparison of the generalized temperature profiles along the centerline of the circular cross-section for the **H1** and **T** boundary conditions.

matrix algorithm (TDMA) (for a review see Patankar, 1980) was employed as the equation solver. The computational result yields Nu_b to 3.65679345, which shows little difference from the infinite series solution of 3.6567935 (Shah and London, 1978). On the other hand, Nu is obtained to 5.154002, which is newly recommended for the circular channel under **T**. Fig. 7 shows the generalized temperature profiles along the centerline of the circular cross-section. Similarly to the square channel, the comparison reveals that the profile for **H1** is more uniform than that of **T**.

5. Conclusion

In this study, it was newly proposed that the Nusselt number based on the fluid mean temperature should be adopted for determining the interfacial heat transfer coefficient in the two-equation porous medium model of the flow-through monolithic catalytic converter. By employing the numerical as well as analytical method, the Nusselt number values were obtained and proposed for practical uses in the square and circular cross-sections under the **H1** and **T** boundary conditions, respectively.

The currently obtained Nusselt numbers based on the fluid mean temperature were approximately 37% to 47 % larger than those based on the fluid bulk mean temperature. This indicates that, in previous studies on modeling automotive catalytic converters, the interfacial heat and mass transfer coefficients have been underestimated up to now.

Notation

a	one-side length of computational domain for square cross-section
a_c	catalyst surface area per unit reactor volume, m^2/m^3
a_{sf}	gas/solid interfacial area per unit reactor volume, m^2/m^3
A	cross-section area, m^2
A_p	pore area of channel, m^2
c_p	specific heat, J/kg/K
C	molar concentration, mol/m^3
d_h	hydraulic diameter of a single channel, m
D	binary diffusion coefficient, m^2/s
f	friction factor
h	heat transfer coefficient based on fluid bulk mean temperature, $W/m^2/K$
h_{sf}	interfacial heat transfer coefficient between gas and solid phases, $W/m^2/K$
$-\Delta H_i$	heat of reaction of species i, J/mol
k	thermal conductivity, W/m/K
k_m	interfacial mass transfer coefficient between gas and solid phases, m/s
K	permeability, m^2
L_{hy}	hydrodynamic entrance length, m
N	number of grid points
Nu	Nusselt number based on fluid mean temperature
Nu_b	Nusselt number based on fluid bulk mean temperature
P	pressure, Pa
q'	heat transfer rate per unit axial length, W/m
q''	heat flux, W/m^2
Q	Volumetric flow rate, m^3/s
r	radial position, m
R_i	reaction rate of species i, $mol/m^2/s$
Re	Reynolds number
Sh	Sherwood number
t	time, s
T	temperature, K
u	velocity, m/s
u_D	superficial velocity (Darcean velocity), m/s
V	volume, m^3
x	axial position, m
y	vertical position for square cross-section, m
z	horizontal position for square cross-section, m

Greek letters

ε	porosity
μ	dynamic viscosity, $N\,s/m^2$
ρ	density, kg/m^3
ϕ	general variable

Subscripts

f	fluid mean property
g	gas phase
i	species horizontal index for square channel (radial index for circular channel)
j	vertical index for square channel
m	fluid bulk mean property
r	radial direction
s	solid phase
x	axial direction

Superscripts

p	previous iteration step
$*$	non-dimensional index for square channel
$+$	non-dimensional index for circular channel

Acknowledgements

This work is part of the project "Development of Partial Zero Emission Technology for Future Vehicle" funded by the Ministry of Commerce, Industry and Energy and we are very grateful for its financial support. Special thanks are also indebted to Dr. D. K. Kim of Applied Heat Transfer Laboratory in Korea Advanced Institute of Science and Technology who provided a valuable discussion on this paper.

References

Asako, Y., Nakamura, H., Faghri, M., 1988. Developing laminar flow and heat transfer in the entrance region of regular polygonal ducts. International Journal of Heat and Mass Transfer 31, 2590–2593.

Bejan, A., 1995. Convective Heat Transfer, second ed. Wiley, New York, pp. 97–118, 121–124, 466–514, 520–523.

Chen, D.K.S., Cole, C.E., 1989. Numerical simulation and experimental verification of conversion and thermal responses for a Pt/Rh metal monolithic converter. SAE Paper 890798.

Chen, D.K.S., Bissett, E.J., Oh, S.H., Ostrom, D.L., 1988. A three-dimensional model for the analysis of transient thermal and conversion characteristics of monolithic catalytic converters. SAE Paper 880282.

Clark, S.H., Kays, W.M., 1953. Laminar-flow forced convection in rectangular tubes. Transactions of the ASME 75, 859–866.

Guojiang, W., Song, T., 2005. CFD simulation of the effect of upstream flow distribution on the light-off performance of a catalytic converter. Energy Conversion and Management 46, 2010–2031.

Incropera, F.P., Dewitt, D.P., 2002. Fundamentals of Heat and Mass Transfer, fifth ed. Wiley, New York, pp. 477–487, 917.

Jeong, S.J., Kim, W.S., 2000. Three-dimensional numerical study on the use of warm-up catalyst to improve light-off performance. SAE Paper 2000-01-0207.

Kaviany, M., 1995. Principles of Heat Transfer in Porous Media, second ed. Springer, New York, pp. 17–20, 391–424.

Kays, W.M., Crawford, M.E., 1993. Convective Heat and Mass Transfer, third ed. McGraw-Hill, New York, pp. 75–87, 108–114, 118.

Keren, I., Sheintuch, M., 2000. Modeling and analysis of spatiotemporal oscillatory patterns during CO oxidation in the catalytic converter. Chemical Engineering Science 55, 1461–1475.

Koltsakis, G.C., Stamatelos, A.M., 1997. Catalytic automotive exhaust aftertreatment. Progress in Energy and Combustion Science 23, 1–39.

Nield, D.A., Bejan, A., 1992. Convection in Porous Media. Springer, New York, pp. 5–14, 35–37.

Oh, S.H., Cavendish, J.C., 1982. Transients of monolithic catalytic converters: response to step changes in feedstream temperature as related to controlling automobile emissions. Industrial and Engineering Chemistry—Product Research and Development 21, 29–37.

Patankar, S.V., 1980. Numerical Heat Transfer and Fluid Flow. Hemisphere, Washington DC. pp. 52–54.

Quintard, M., Whitaker, S., 2000. Theoretical analysis of transport in porous media. In: Vafai, K., Hadim, H.A. (Eds.), Handbook of Porous Media. Marcel Dekker, New York. pp. 4–6.

Shah, R.K., 1975. Laminar flow friction and forced convection heat transfer in ducts of arbitrary geometry. International Journal of Heat and Mass Transfer 18, 849–862.

Shah, R.K., London, A.L., 1974. Thermal boundary conditions and some solutions for laminar duct flow forced convection. Journal of Heat Transfer 96, 159–165.

Shah, R.K., London, A.L., 1978. Laminar Flow Forced Convection in Ducts, Supplement to Advances in Heat Transfer. Academic Press, New York, pp. 78–79, 196–203.

Siemund, S., Leclerc, J.P., Schweich, D., Prigent, M., Castagna, F., 1996. Three-way monolithic converter: simulations versus experiments. Chemical Engineering Science 51, 3709–3720.

Stone, H.L., 1968. Iterative solution of implicit approximations of multidimensional partial differential equations. SIAM Journal on Numerical Analysis 5, 530–558.

Taylor, W., 1999. CFD prediction and experimental validation of high-temperature thermal behavior in catalytic converters. SAE Paper 1999-01-0454.

Wiginton, C.L., Dalton, C., 1970. Incompressible laminar flow in the entrance region of a rectangular duct. Journal of Applied Mechanics 37, 854–856.

Zygourakis, K., 1989. Transient operation of monolith catalytic converters: a two-dimensional reactor model and the effects of radially nonuniform flow distributions. Chemical Engineering Science 44, 2075–2086.